Dynamics of Hydration Water on Rutile Studied by Backscattering Neutron Spectroscopy and Molecular Dynamics Simulation

E. Mamontov,*,† D. J. Wesolowski,‡ L. Vlcek,§ P. T. Cummings,§,‖ J. Rosenqvist,‡ W. Wang,⊥ and D. R. Cole‡

Spallation Neutron Source, Oak Ridge National Laboratory, Oak Ridge, Tennessee 37831-6473, Chemical Sciences Division, Oak Ridge National Laboratory, Oak Ridge, Tennessee 37831-6110, Department of Chemical Engineering, Vanderbilt University, Nashville, Tennessee 37235-1604, Center for Nanophase Materials Sciences, Oak Ridge National Laboratory, Oak Ridge, Tennessee 37831-6496, and Environmental Sciences Division, Oak Ridge National Laboratory, Oak Ridge, Tennessee 37831-6036

Received: December 20, 2007; Revised Manuscript Received: June 4, 2008

The high energy resolution, coupled with the wide dynamic range, of the new backscattering spectrometer (BASIS) at the Spallation Neutron Source, Oak Ridge National Laboratory, has made it possible to investigate the diffusion dynamics of hydration water on the surface of rutile (TiO_2) nanopowder down to a temperature of 195 K. The dynamics measured on the BASIS on the time scale of tens of picoseconds to more than a nanosecond can be attributed to the mobility of the outer hydration water layers. The data obtained on the BASIS and in a previous study using the backscattering and disk-chopper spectrometers at the NIST Center for Neutron Research are coupled with molecular dynamics simulations extended to 50 ns. The results suggest that the scattering experiments probe several types of molecular motion in the surface layers, namely a very fast component that involves dynamics of water molecules with unsaturated hydrogen bonds, a somewhat slower component due to localized motions of all water molecules, and a much slower component related to the translational jumps of the fully hydrogen-bonded water molecules. The temperature dependence of the relaxation times associated with the localized dynamics remains Arrhenius down to at least 195 K, whereas the slow translational component shows non-Arrhenius behavior above about 205 K. Thus, an Arrhenius-type behavior of the faster localized dynamic component extends below the temperature of the dynamic transition in the slow translational component. We suggest that the qualitative difference in the character of the temperature dependence between these slow and fast components may be due to the fact that the latter involves motions that require breaking fewer hydrogen bonds.

1. Introduction

Quasielastic neutron scattering (QENS) was instrumental in the recent observations of a dynamic transition in confined water when supercooled below its homogeneous nucleation temperature.[1–3] Below the transition temperature of ≈220 K, the temperature dependence of the measured relaxation time in water changes from a high-temperature non-Arrhenius-type to a low-temperature Arrhenius-type. The original explanation for this dynamic transition, which was supported by molecular dynamics (MD) simulations,[4] is that the crossover in the water dynamics corresponds to the "fragile"-to-"strong" liquid transition predicted a decade ago.[5] In this interpretation, the dynamic transition reflects the structural changes due to a transformation from a high-density, high-temperature, liquid phase to a low-density, low-temperature, liquid phase having a much more developed hydrogen bond network. More recently it has been argued that the observed dynamic transition could also be due to a confinement-induced vanishing of the α-relaxation in water, which leaves only a β-relaxation that is characterized by an Arrhenius behavior.[6] While the nature of the dynamic transition is actively debated, its presence has been found in QENS experiments on water confined in various systems, such as carbon nanotubes,[7] oxide nanopowder surfaces,[8,9] and hydration water in lysozyme[10] and DNA.[11] The latter experiments appear to support a conjecture that it is the change of mobility in the hydration water that triggers the onset of the dynamic transition and the related bioactivity in proteins and other biomolecules.[10,11]

Oxide surfaces are attractive for studying the dynamics of hydration water because of their relative simplicity compared to biosurfaces, which allows detailed molecular dynamics simulations for interpretation of the experimental data. For example, in our recent QENS-MD study[9] we have identified three distinct hydration layers on the (110) crystal surface of rutile (α-TiO_2), L_1, L_2, and L_3, characterized by different structures and dynamics (see Figure 1). The diffusion dynamics of hydration water on rutile on the nanosecond time scale was studied on the High Flux Backscattering Spectrometer (HFBS) at the NIST Center for Neutron Research (NCNR) and exhibited a transition from high-temperature non-Arrhenius behavior between 220 and 210 K.[9] Faster dynamics, on the time scale of tens of picoseconds or less, were investigated on the Disk Chopper Spectrometer (DCS) at the NCNR and exhibited two separate components, both of which appeared Arrhenius down to the lowest measurement temperature of 250 K.[9] These faster dynamics could not however be investigated in the DCS experiment below 250 K because of insufficient energy resolution. Likewise, these faster dynamics could not be adequately

* To whom correspondence should be addressed. E-mail: mamontove@ornl.gov. Phone: (865) 574-5109. Fax: (865) 574-6080.
† Spallation Neutron Source, Oak Ridge National Laboratory.
‡ Chemical Sciences Division, Oak Ridge National Laboratory.
§ Vanderbilt University.
‖ Center for Nanophase Materials Sciences, Oak Ridge National Laboratory.
⊥ Environmental Sciences Division, Oak Ridge National Laboratory.

10.1021/jp711965x CCC: $40.75 © 2008 American Chemical Society
Published on Web 07/17/2008

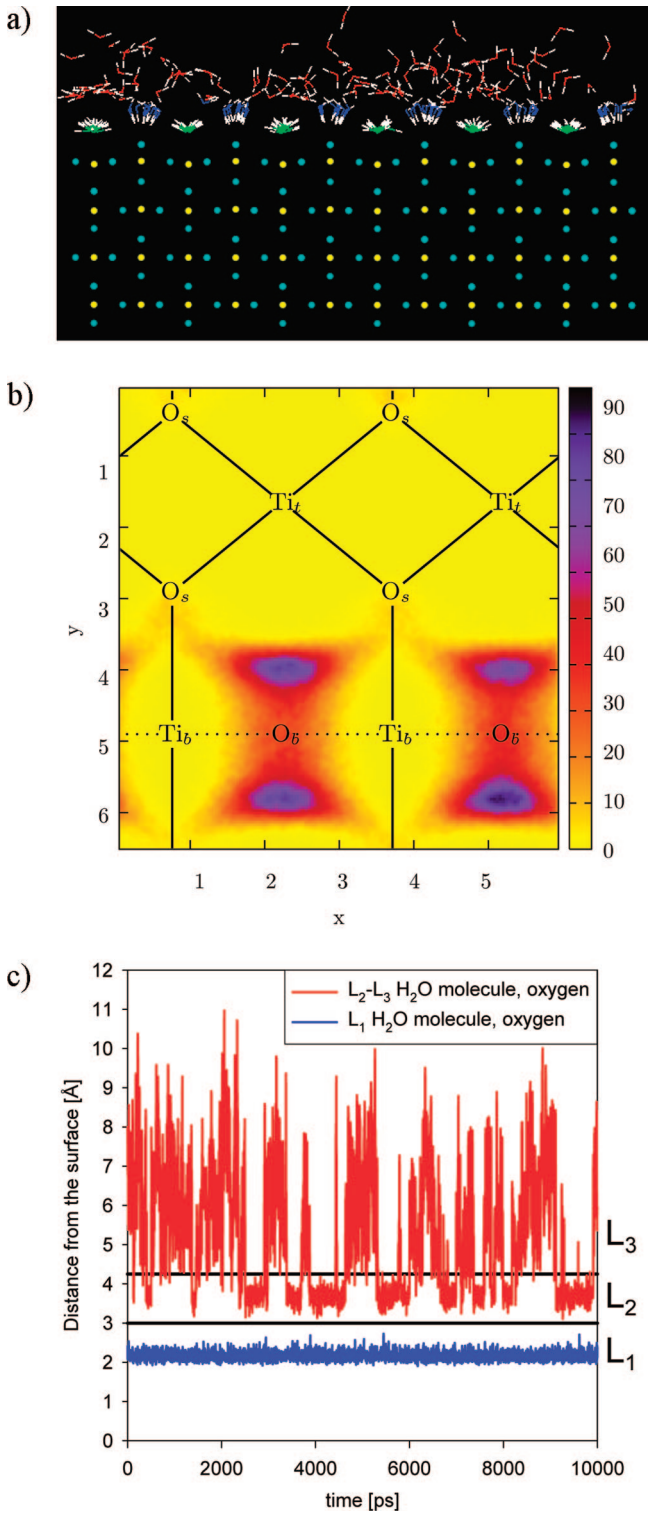

Figure 1. (a) MD snapshot of rutile hydrated surface.[9] Titanium atoms: yellow. Oxygen atoms in rutile: cyan. Oxygen atoms in the L_1 layer: green. Oxygen atoms in the L_2 layer: blue. Oxygen atoms in the L_3 layer: red. Hydrogen: white. (b) The lateral density distributions of oxygen atoms of hydration water in the L_2 layer. The positions of rutile surface Ti and O atoms are denoted by corresponding symbols. Subscripts "b", "t", and "s" denote bridging, terminal, and in-surface (as opposed to protruding bridging and terminal) atoms, respectively. (c) The distance from the TiO_2 surface as a function of time for the oxygen atoms of two arbitrarily selected water molecules (one from the L_1 layer, the other from the L_2-L_3 layers).

studied in the HFBS experiment because of the limited dynamic range of that instrument. These limitations have left the following important question unanswered: do the faster diffusion dynamics show a dynamic transition similar to the one exhibited by the slow diffusion component?

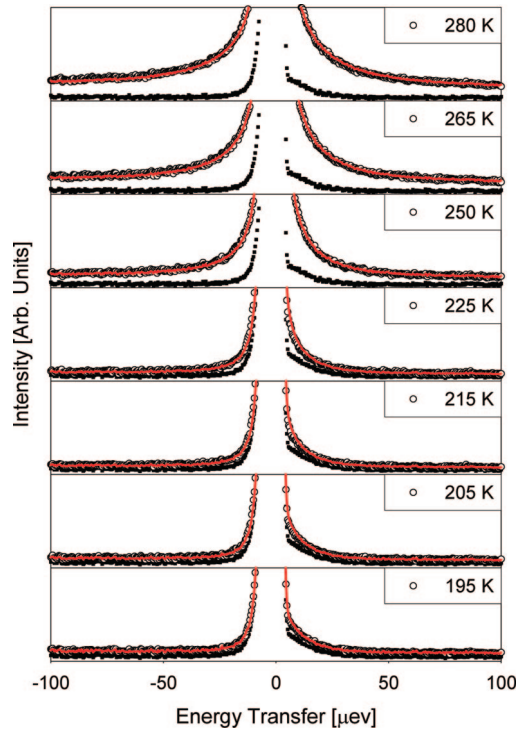

Figure 2. Temperature dependence of the scattering intensities (open symbols). The resolution functions are shown with filled symbols. The solid lines show fits obtained using eqs (1) and (2) for $-200\ \mu eV < E < 800\ \mu eV$. The elastic intensities and the energy transfer range shown in the figure are truncated to emphasize the QENS signal.

In order to address this question, we used the new backscattering spectrometer at the Spallation Neutron Source (SNS) at Oak Ridge National Laboratory (ORNL) that uniquely possesses both a sufficiently high energy resolution and a sufficiently wide dynamic range to probe the dynamics of hydration water on rutile to a low temperature of 195 K.

2. Experimental Section

The rutile nanopowder synthesis, hydration, and characterization, as well as molecular dynamics simulations of SPC/E water on the rutile surface have been described in great detail elsewhere,[9] and we will not therefore repeat the description here. Figure 2 of our previous paper[9] clearly shows that the rutile nanoparticles synthesized for our QENS studies consist of radiating clusters of individual single-crystal nanoparticles with a rod-like shape, and aspect ratio (length/diameter) ranging from 5 to 10. As shown, high-resolution transmission microscopy analysis demonstrates that the crystal planes parallel to the long axis of the rods exhibit the 0.32 nm *d*-spacing characteristic of rutile (110) planes. In fact, this is entirely characteristic of rutile nanoparticles synthesized by a variety of techniques similar to that used to prepare our samples,[12–14] and even macroscopic rutile particles, such as the Tioxide Corp. rutile used in many of our previous investigations of rutile surface charge and ion adsorption.[15] The extremely simple morphology of hydrothermally synthesized nanorutile is well demonstrated by the excellent transmission electron microscopy studies of Huang and Pan,[13] who demonstrate that the (110) surface has the lowest surface energy of all the common surfaces developed on rutile nanorods, thus promoting elongation in the direction perpen-

dicular to (110), resulting in rectangular growth prisms with typically >70% of their surface area composed of the (110) surface. Furthermore, Jones and Hockey[16] long ago demonstrated that bridging and terminal oxygen atoms are the predominant protolytic sites on the other common growth surfaces or rutile (100 and 111), and these same surface sites on (110) are shown to be the only active sites for proton and ion adsorption, as well as hydrogen bonding with adsorbed water molecules, from our extensive X-ray, SHG and computational studies.[17–19] From these observations, we conclude that there is little to be gained by simulating water dynamics on rutile surfaces other than the (110) surface in order to link the MD results with our QENS studies of the dynamics of water on rutile nanopowders with the (110) face predominant, particularly because the QENS signal averages the contributions from all water molecules, and will be dominated by water on the predominant crystal face. The extensive validation of our ab initio-optimized classical MD simulations of water on this surface[20,21] argues strongly in favor of the use of this MD model for comparison with QENS measurements on our hydrated rutile nanoparticles.

For this study, the MD simulations were extended to a much longer time (50 ns) and subjected to additional analyses, as will be discussed below, but the simulation methodology is the same as in the previous paper.[9] However, because the current work describes early scientific results obtained on the new backscattering spectrometer at the SNS, we will address the description of our neutron scattering measurements in some detail.

The Backscattering Silicon Spectrometer (BASIS) is an inverse geometry time-of-flight spectrometer that uses Si(111) analyzer crystals to select the final energy of 2082 μeV (6.267 Å) for neutrons scattered by a sample illuminated by a polychromatic neutron beam, the bandwidth of which is defined by a set of neutron choppers.[22] When the instrument choppers are operated at the design frequency of the SNS accelerator, 60 Hz, a dynamic range of more than $\pm$ 200 μeV is accessible. The dynamic range can be further extended by operating the choppers at lower frequency. In this study, we operated the choppers at 15 Hz (matching the current accelerator frequency). For the data analysis, we selected a dynamic range from -200 μeV to $+800$ μeV.

The rutile nanopowder, which was pre-equilibrated with the laboratory atmosphere (~75% relative humidity at ~23 °C), was loaded into a 1 mm wide annular space between two cylindrical aluminum surfaces, with an outer diameter of 30 mm. Both the sample container and the sample preparation were identical to those employed in our previous studies at the HFBS spectrometer at the NCNR.[9] With a sample diameter of 30 mm, and combining data across the Q-range measured on the BASIS, we achieved a resolution at the elastic line of 3.3−3.6 μeV (full width at half-maximum, fwhm), depending on the state of the hydrogen moderator that provides neutrons to the spectrometer. The sample configuration was chosen to ensure greater than 90% neutron beam transmission through the sample in order to minimize the effects of multiple scattering. The aluminum sample container was mounted onto a closed-cycle refrigerator, which controlled the temperature within ±0.5 K. The data were collected at 280, 265, 250, 225, 215, 205, and 195 K. In addition, two sets of data have been collected from the sample at 7.2 K before and after this series of measurements and used as resolution functions. This was done because the hydrogen moderator was refilled in the middle of the temperature series, and we had to ensure that the data at each temperature point were analyzed in conjunction with the resolution function representing the state of the moderator before and after the refill.

In order to maximize the signal-to-background ratio, we used only the detectors spanning the in-plane scattering angles from 33° to 123°, which corresponds to 0.57 Å^{-1} < Q < 1.76 Å^{-1} (at the elastic channel). Similar to the data treatment applied in the earlier study,[9] we summed up the data over the entire Q range. It should be noted that analysis of the Q-dependence of the QENS signal would be complicated due to somewhat limited data statistics since the experiment was carried out at the SNS accelerator power of 40−60 kW, which is less than 5% of the baseline target power of 1.4 MW. Fortunately, as we have discussed in the earlier study,[9] due to spatially restricted character of molecular motions, QENS signal from this system shows only a weak Q-dependence in the temperature range and Q-range that we probed, which makes analyzing Q-averaged data possible. The width of the Q-averaged QENS signal is inversely proportional to the characteristic relaxation time. A weak Q-dependence of the relaxation times for 0.57 Å^{-1} < Q < 1.76 Å^{-1} has been independently confirmed by our MD simulations.

The data were converted from the time-of-flight bins to incident wavelength bins and normalized by the efficiency-corrected signal of the incident beam monitor. The scattering signal from the empty sample holder was processed in the same way and subtracted from the data. The resulting data were converted from the wavelength bins to energy transfer bins of 0.4 μeV width. The output of the data reduction procedure was proportional to the Q-averaged differential scattering cross-section. In order to simplify the treatment of the background signal, no further corrections were applied to the data. Instead, the kinematic factor of k_f/k_i and the temperature-dependent detailed balance factor were incorporated in the model scattering function, $S(E)$, used in the data analysis.

3. Results and Discussion

3.1. Quasielastic Neutron Scattering. Following the previously adopted procedure,[9] the data were fit using the expression

$$I(E) = [x\delta(E) + (1-x)S(E) + B(E)] \otimes R(E) \qquad (1)$$

Here $\delta(E)$ is a delta function centered at zero energy transfer, x represents the fraction of the elastic scattering, $B(E)$ is the background term, $R(E)$ is the resolution function, and $S(E)$ is the model scattering function in the form of

$$S(E) = \left[(1-p)\frac{1}{\pi}\frac{\Gamma_1}{E^2+\Gamma_1^2} + p\frac{1}{\pi}\frac{\Gamma_2}{E^2+\Gamma_2^2}\right]\left(\sqrt{\frac{E_0}{E+E_0}}\right)\times \exp\left(\frac{E}{2kT}\right) \qquad (2)$$

where the elastic energy $E_0 = 2082$ μeV, k is the Boltzmann's constant, and T is the sample temperature. The term in the second bracket is the kinematic factor of k_f/k_i, and the exponential term describes the temperature-dependent detailed balance. Explicit incorporation of these factors into the model scattering function rather than their application in the course of the data reduction assures that they do not affect the background term. The two-Lorentzian term in the first bracket includes a faster (broader) and a slower (narrower) diffusion component. Even though one can use a different function, for instance, in the form of a Fourier-transformed stretched exponential, we have decided to use the two-Lorentzian function for several reasons. First, with a fit background, the BASIS data could be adequately fit with only two components, as we will discuss below. Second,

TABLE 1: Comparison of the Relaxation Times (in ps) for Hydration Water in Rutile Obtained in the Earlier Study[9] Using the Disk Chopper Spectrometer (DCS) at the NCNR and in the Current Study Using the BASIS[a]

T, K	DCS fast component	DCS slow component	BASIS fast component	BASIS slow component	HFBS
345	3.90 (0.39)	23.10 (1.40)			
320	4.32 (0.48)	24.90 (1.50)			
300	5.28 (0.63)	29.68 (2.04)			
280	4.95 (0.90)	33.60 (2.19)	24.32 (0.47)	177.80 (3.47)	630 (28)
265			30.33 (0.88)	209.22 (5.70)	
260					659 (25)
250	6.42 (3.60)	46.41 (7.07)	31.24 (1.34)	222.97 (6.02)	
240					787 (27)
225			72.18 (7.12)	656.24 (71.51)	
220					1254 (72)
215			76.97 (7.37)	1068.87 (131.31)	
210					1513 (150)
205			110.48 (9.55)	2521.88 (318.18)	
200					1382 (227)
195			111.86 (11.53)	3563.68 (361.19)	

[a] The relaxation times are calculated as $\tau = \hbar/\Gamma$, where Γ is the HWHM of the Lorentzian broadening obtained using eqs 1 and 2. The standard deviation values are shown in parenthesis.

eq 2 was used in order to perform a direct comparison with the previous results,[9] which were analyzed using the two-Lorentzian functional form. Finally, a fit with a single stretched exponential would contradict the MD results that suggest the presence of several distinct dynamic components, while fitting data with more than one stretched exponential component rarely produces sound results.

In Eq. 1, we used the background term in the form of $B(E) = C_1 + C_2(E + E_0)^{-3/2}$, where the elastic energy $E_0 = 2082$ μeV as mentioned above. This functional form accounts for both processes on a faster time scale and a possible constant (but sample- and temperature-dependent) background in time-of-flight, which, upon conversion to energy transfer, E, would yield the component proportional to $(E + E_0)^{-3/2}$. Since the precise evaluation and subtraction of the time-of-flight background in our experiment was difficult, it was more practical to use the nonlinear background term for the data fits.

The temperature dependence of the data and fits are presented in Figure 2. The horizontal axis in Figure 2 is limited to ± 100 μeV in order to illustrate the QENS broadening at low temperatures more clearly, but the fits were performed for the much broader range of -200 μeV $< E <$ 800 μeV. The decrease in both the relative strength and width of the QENS signal as the temperature is decreased is evident, indicating slower motions at lower temperatures.

The temperature dependence of the relaxation times obtained in the current experiment on the BASIS and calculated from the Lorentzian half-width at half-maximum (HWHM), Γ, as $\tau = \hbar/\Gamma$ is presented in Table 1 and Figure 3. The relaxation times obtained from the data collected in the previous experiments[9] on the DCS and HFBS are shown for comparison. It should be noted that we did not make assumptions concerning the origin of particular components; for instance, we did not assume that the fast components are due to hindered isotropic rotational jumps, for which $\tau = \hbar/3\Gamma$.

The fast BASIS component exhibits an Arrhenius-type temperature dependence down to 195 K and shows reasonable agreement with the slow DCS component in the temperature range where the BASIS and DCS measurements overlap. Since the dynamic ranges of the BASIS and DCS measurements are similar (-200 to $+800$ and $\pm$ 500 μeV, respectively), this agreement is expected and shows the consistency between the two experiments. Furthermore, the BASIS data were also analyzed by including a third, very fast component obtained

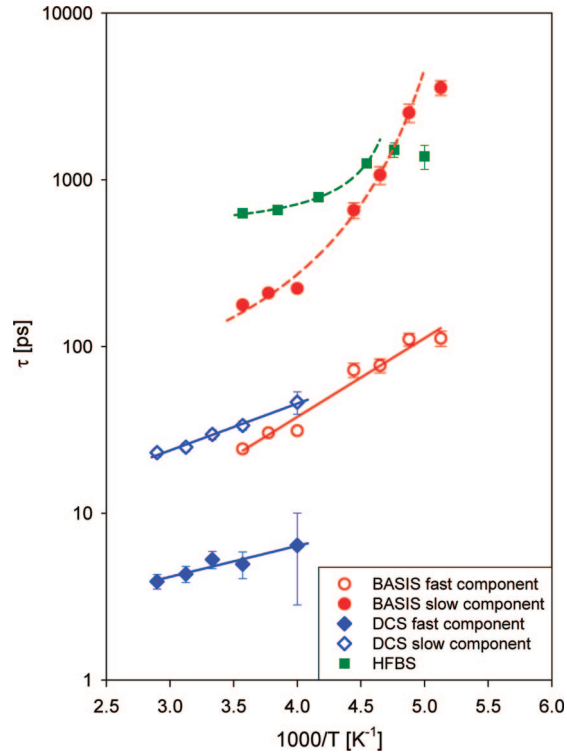

Figure 3. Temperature dependence of the relaxation times calculated as $\tau = \hbar/\Gamma$, where Γ is the HWHM of the Lorentzian broadening obtained using eqs 1 and 2. The Arrhenius fits of the fast components (solid lines) yield activation energies of 3.6 $\pm$ 0.7, 5.4 $\pm$ 0.3, and 9.0 $\pm$ 0.8 kJ/mol for the DCS fast, DCS slow, and the BASIS fast component, respectively. Also shown (dashed lines) are the VFT fits obtained using the six higher temperature points of the BASIS slow component and the four higher temperature points of the HFBS data.

by extrapolating the very fast DCS component over the temperature range of the BASIS experiment. No significant improvement in the fit to the BASIS data was obtained by this procedure, and the relaxation times obtained for the two free components were virtually the same as those obtained from the two-Lorentzian fits; however, this demonstrates that the BASIS results are consistent with the previous results for the two DCS components plotted in Figure 3. Three-Lorentzian fits of the BASIS data with all free components could not resolve the very fast component, likely because of the relatively high background

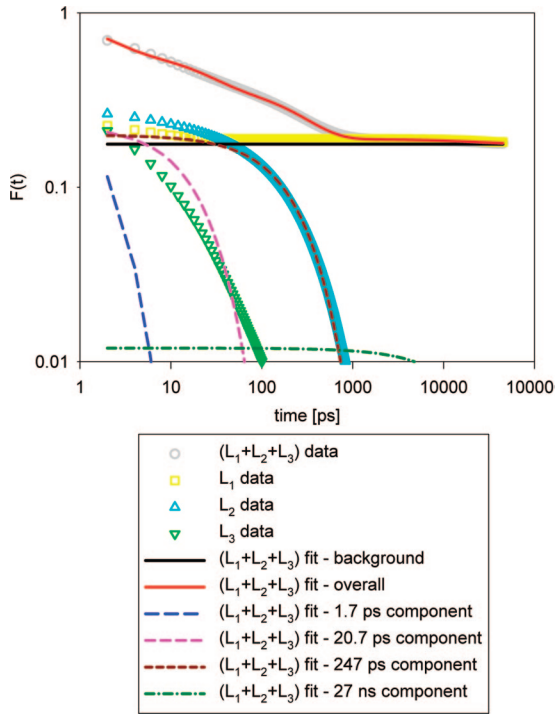

Figure 4. Intermediate scattering function, $F(t)$, obtained in the MD simulation of the hydration water in TiO_2 at 300 K for the entire system of hydration water ($L_1 + L_2 + L_3$) and for the separate hydration layers. The $F(t)$'s for the separate layers are weighed for the fraction of water molecules occupying a particular layer in such a way that a sum of individual layer $F(t)$'s yields the total $F(t)$. Also shown are the overall fit of the ($L_1 + L_2 + L_3$) data and its individual components (four exponential decays and a flat background).

in the BASIS data that we had to model using a nonlinear term as explained above.

The slow BASIS component shows some faster relaxation times at higher temperatures compared to the HFBS data. The difference in the relaxation times between the HFBS and BASIS data is likely due to better energy resolution and, more importantly, limited dynamic range of the former spectrometer. It is not uncommon for systems with a distribution of relaxation times to show a dependence of the measured relaxation time on the resolution of the measurement.[23] In fact, the MD data may suggest the potential source of the difference between the HFBS and BASIS data at higher temperatures, as we will discuss below. However, importantly, the data from both spectrometers exhibit qualitatively similar behavior, showing non-Arrhenius character at higher temperatures (VFT fits of relaxation times, $\tau = \tau_0 \exp(DT_0/(T - T_0))$, yield $T_0 = (201 \pm 4)$ K and (165 ± 6) K for the HFBS and BASIS data, respectively) and deviations from the VFT law at lower temperatures.

3.2. Molecular Dynamics Simulation. For this study, the MD simulations of the hydration water on rutile (110) crystal surface at 300 K similar to those described in the previous work[9] were extended from 10 to 50 ns. The simulations were carried out at approximately the same surface water coverage as determined experimentally for the hydrated rutile nanopowder used in this and the previous[9] QENS studies, nearly full three-layer coverage, with the layers defined by MD to contain on average 1.0 (L_1), 1.07 (L_2) and 1.43 (L_3) water molecules per Ti_2O_4 surface unit. The results of the MD simulations are presented in Figures 1 and 4.

The simulations showed that the structure and dynamics of the L_1 and L_2 layers are dictated primarily by strong bonds to the metal atoms and surface oxygen atoms, respectively, which localize the water molecules of these hydration layers and prevent lateral motion. The clear separation of water molecules of the L_1 layer from the rest of the system seen in Figure 1a indicates that there may be only a very limited diffusion involving molecules of this layer. Highly localized peaks seen in the lateral density profiles of water in L_2 (Figure 1b) also suggest that there will be little to no diffusive motions within this layer. However, unlike the water molecules of the L_1 layer, those belonging to the L_2 layer may contribute to diffusivities through the exchange with the L_3 layer water molecules. This is illustrated by Figures 1c and 4 and will be discussed in detail below. Finally, the water molecules of the L_3 layer are delocalized in the lateral directions. This is consistent with their high mobility, as we will discuss below.

The intermediate scattering function, $F(t)$, in Figure 4 representing the dynamics of the entire system, $L_1 + L_2 + L_3$, shows at least three major and one very minor distinct dynamic components. A fit with a sum of four exponential decays and a flat background (the latter representative of very slow moving or static water molecules) yields the relaxation times of 1.7 ps, 20.7 ps, 247 ps, and 27 ns. The faster three of these four components are within the range accessible in our QENS measurements, and they have been already investigated in our previous work.[9] These components are related to the distinct dynamic processes that manifest themselves in our QENS results plotted in Figure 3: one on the picosecond time scale, represented by the fast DCS component, the other on the tens of picoseconds time scale, represented by the slow DCS component and fast BASIS component, and, finally, the slow dynamics on the time scale of hundreds of picoseconds to a nanosecond, represented by the HFBS and slow BASIS component. The slowest dynamic component in the MD $F(t)$ with residence times on the time scale of tens of nanoseconds has not been seen in the earlier shorter MD simulations; neither has it contributed significantly to the scattering signal in our QENS experiments. Qualitative examination of our MD data suggest that this very slow motion is related to rare escapes of L_1 water molecules chemisorbed to undercoordinated surface Ti atoms, as depicted for the (110) crystal surface in Figure 1a.

In addition to the overall dynamics of the system, in the current MD simulation we were able to investigate the dynamics of the three hydration layers separately (Figure 4). It should be noted that the MD simulations in our previous study[9] have demonstrated that the molecules of the L_2 and L_3 layers undergo exchange on the time scale of the QENS experiments. Thus, when discussing the dynamics of a separate layer, we refer to the dynamics of molecules that currently reside in that particular layer, irrespective of their previous or subsequent locations.

As one can see in Figure 4, the innermost hydration layer, L_1, accounts for the entire background in the overall $F(t)$, whereas its contribution to the dynamics of the overall $F(t)$ is very small. A small decay in the $F(t)$ of L_1 at short relaxation times is due to localized motions of the L_1 water molecules. Even smaller decay at very long relaxation times (tens of picoseconds) is related to very infrequent translational jumps of the L_1 molecules. This type of dynamics is too slow and of low statistics to be adequately assessed even in the 50 ns long MD simulation, and is definitely far outside the range of the QENS experiments, contributing only to the elastic signal in all spectrometers. Overall, the L_1 layer shows very limited mobility, and its contribution to the QENS signal and the MD data at times shorter than a nanosecond is small. The dynamics observed in our QENS experiments almost entirely originate from the mobility of the outer L_2 and L_3 hydration layers.

TABLE 2: Comparison of the Fits of the MD Data for the L_3 and L_2 Hydration Layers Obtained Using Three Exponential Decays

	component 1		component 2		component 3	
	weight, %	relaxation time, ps	weight, %	relaxation time, ps	weight, %	relaxation time, ps
L_2	25	4.7	32	107.1	43	327.2
L_3	55	1.4	40	15.5	5	141.7

The MD dynamics of L_2 at relaxation times of 100 ps and above are very accurately described by a single exponential decay (Figure 4). These dynamics are due to relatively slow translational jumps of fully hydrogen-bonded water molecules and are related to the QENS signal observed in the HFBS experiment and as the slow component in the BASIS experiment. Even though the QENS measurements probe only the dynamics of the hydrogen atoms in the system, our MD simulations enable analysis of the dynamics of oxygen atoms as well. Diffusion dynamics of hydrogen atoms arise from both translational and rotational motions of the water molecules. Thus, truly translational motions can be better defined by analyzing the dynamics of the oxygen atoms, as shown in Figure 1c. The oxygen atom of an L_1 molecule is essentially fixed (at least within the time frame of the QENS measurements) in its sorption site above a 5-coordinated Ti atom at the crystal surface. On the other hand, an L_2 oxygen atom resides for extended periods of time in its constrained sorption site above the crystal surface, where the water molecules form strong hydrogen bonds with the L_1 water molecules and the bridging oxygen atoms of the crystal surface, but it also escapes occasionally into the L_3 layer and resides there for extended periods of time as well, undergoing large displacements within this outermost layer. Because L_2 is composed almost entirely of water molecules that lie between the rows of L_1 molecules and rows of bridging surface oxygen atoms, the translational jumps within L_2 are hindered. However, the translational jumps from L_2 to L_3, which occur on the time scale of hundreds of picoseconds, as one can see in Figure 1c, contribute to the slow component of the $F(t)$ observed in the MD simulation and QENS experiments (HFBS and slow BASIS component). The L_2 layer also exhibits faster relaxation dynamics at times shorter than 100 ps, which are mainly due to hindered localized motions of its water molecules that involve breaking fewer than three hydrogen bonds and no escape from the cage of the neighboring water molecules. Indeed, between the translational jumps, the motions of the L_2 water molecules are localized, as evidenced by the relatively immobile oxygen atoms (Figure 1c). These motions contribute to the faster component of the $F(t)$ observed in the MD simulation and QENS experiments (slow DCS and fast BASIS components).

On the other hand, the dynamics of the L_3 are significantly faster compared to the L_2 and are mostly observed below 100 ps. The L_3 dynamics comprise two fast components, on the time scale of picoseconds and tens of picoseconds. To emphasize the difference between the L_3 and L_2, Table 2 shows the results of fitting the MD data for these layers using a sum of weighed exponential decays, $F(t) = C_1 \exp(-t/\tau_1) + C_2 \exp(-t/\tau_2) + C_3 \exp(-t/\tau_3)$, where $C_1 + C_2 + C_3 = 1$. Not only the relaxation times for the components of L_3 are significantly faster, but also the spectral weight of the fast components dominates the L_3 dynamics. For example, the slowest of the three exponential components, on the time scale of hundreds of picoseconds, contributes 43% to the fit of the L_2 dynamics, but only 5% to the fit of the L_3 dynamics. Thus, the slow translational jumps dominate the L_2 dynamics, but carry little spectral weight in the L_3 dynamics. On the other hand, the L_3 dynamics is dominated by the fast components, whose contribution to the L_2 dynamics is substantially lower. We attribute the high weight of the fast components in the L_3 dynamics to the fact that, in addition to hindered localized motions, observed in L_2 and even in L_1, the molecules of the L_3 can also perform very fast motions because of the low number of hydrogen bonds that they form with the nearest neighbors (based on the MD results, 3.0 on average). These motions represent a distinct feature of the L_3 and are associated with picosecond time scale dynamics which we have previously observed in our DCS experiment.

The fact that the dominant contributions from the L_2 and L_3 layers do not seem to have a strongly stretched character, as evidenced by the MD simulation, justifies using a superposition of Lorentzians for our QENS data analysis. In fact, for our system, where several distinctive dynamic components are present, fitting the QENS data with a superposition of stretched exponentials in the time space (or its Fourier-transform in the energy space) would easily yield unphysical results, because a fit of the experimental data with more than one stretched exponential is rarely sound.

There are several observations that may suggest the potential source of the difference in the relaxation times obtained on the HFBS and BASIS at higher temperatures. In this temperature region, there is a good agreement between the BASIS and molecular dynamics data, whereas the HFBS relaxation times are longer by about a factor of 2−2.5, as one can see from comparison of the 280 K data in Table 1 and the 247 ps component depicted in Figure 4. The overall $F(t)$ plotted in Figure 4 exhibits a transition region at about 1 ns. In particular, at times longer then a nanosecond, the $F(t)$ is no longer dominated by the L_2 dynamics, but instead by the very slow dynamics of the L_1. Based on these observations, one can conclude that it is the HFBS that likely overestimates the relaxation times of the L_2 at the higher measured temperatures because, due to its higher energy resolution compared to the BASIS, it samples some slower part of the L_2 dynamics and some faster part of the L_1 dynamics. On the other hand, the BASIS likely probes the L_2 dynamics, but not the L_1 dynamics; thus it shows a much better agreement with the MD results for the L_2. The HFBS energy resolution corresponds to relaxation times longer than a nanosecond, where the transition from the L_2-dominated dynamics to the L_1-dominated dynamics takes place, as one can see in Figure 4.

As illustrated by Figure 12 of our previous paper,[9] all of the water molecules in our sample exhibit some axial (perpendicular to the surface) structure (even the L_3, albeit to a lesser extent) due to the presence of the rutile surface and strongly layered structure of hydration water. On the other hand, the lateral structure is exhibited by the water molecules of the L_1 and L_2 layers only. The high diffusivity and lateral order appear to be mutually exclusive, as evidenced by the structure and dynamics of the L_3 hydration layer.

3.3. Slow and Fast Dynamic Components. In previous QENS studies of hydration water on various surfaces, including hydrated rutile,[7–11] a dynamic transition from a high-temperature non-Arrhenius behavior to a low-temperature Arrhenius behavior has been found using backscattering spectrometry data obtained with a small dynamic range and sub-μeV resolution that corresponds to the time scale of a nanosecond and longer. The non-Arrhenius behavior seems to be a common feature for the inner hydration water in various systems. For instance, the translational dynamics of water measured in an aqueous solution

of various concentrations of the *N*-acetyl-leucine-methylamide hydrophobic peptide,[24] which has a surface very different from the hydrophilic surface of rutile, has demonstrated strongly non-Arrhenius temperature dependence in the more concentrated solution, where the water molecules are in close contact with the surface, similar to the L_2 layer on rutile. On the other hand, the mobility of water may differ between the L_3 and L_2 layers, as was suggested by the specific heat measurements of surface water on TiO_2 nanoparticles.[25] Until now, the diffusion dynamics of the water molecules on oxide surfaces on a time scale faster than a nanosecond could be probed only at relatively high temperatures, where it appeared to be of an Arrhenius-type.[9,26] Similarly, Arrhenius-type dynamics were observed in monolayers of surface water,[27,28] also at relatively high temperatures. It has been suggested[26,29] that the dynamics associated with the motions of the hydration water molecules that do not escape from the nearest-neighbor cage may remain of an Arrhenius-type even below the temperature of the dynamic transition. On the other hand, if such dynamics are characterized by non-Arrhenius behavior, the true character of the temperature dependence could become visible only at lower temperatures. Until now, the experimental investigation of the faster diffusion component near and below the temperature of the dynamic transition of the slower diffusion component was hampered by the lack of QENS measurements performed with sufficient (μeV-range) resolution and wide enough (tens or hundreds of μeV) dynamic range, for which the BASIS is specifically designed and well-suited.[22] Based on the current BASIS experiment and the MD simulation, one can conclude that the slower, translational component is non-Arrhenius at higher temperatures and exhibits a dynamic transition at lower temperatures, whereas the faster component is Arrhenius and remains such even below the temperature of the dynamic transition of the slower component. The very fast component, which we attribute to the fast dynamics of the underbonded water molecules in the L_3 layer, appears Arrhenius in character at temperatures down to at least 250 K. Whether or not these motions, attributed to the water molecules with significantly less than 4 hydrogen bonds per molecule, are truly Arrhenius at temperatures near and below the dynamic transition of the inner hydration water, remains to be tested experimentally.

The character of the temperature dependence of the dynamic components in the hydration water seems to be similar to that known for bulk water,[30] where the water molecules form, on average, four hydrogen bonds with the nearest neighbors. The faster localized motions in bulk water originating from simultaneous breaking of less than three hydrogen bonds are known to be of Arrhenius-type,[30] whereas the slower translational motion that requires simultaneous breaking of at least three hydrogen bonds is strongly non-Arrhenius.[30] The same consideration should apply to the qualitative difference in the temperature dependence between the fast and slow dynamic components in the hydration water. The slow component, which involves the translational jumps of the fully hydrogen-bonded molecules, is due to motions that require simultaneous breaking of several hydrogen bonds, and possesses the characteristic attributes (non-Arrhenius behavior and dynamic transition) of bulk water translational dynamics. On the other hand, the fast component is Arrhenius because it originates from the localized motions that require breaking fewer hydrogen bonds. It should be noted that the dynamic transition discussed above has been only observed in nanoconfined water within mesoporous media, with confining walls composed of amorphous silica and other discrete molecular phases. The question of whether or not this transition is a feature of nanoconfinement, or an intrinsic feature of water, remains controversial.[31,32]

Based on our studies, we suggest that the reason why there is a distinctive slow translational diffusion component in the system of hydration water on rutile that includes three hydration layers is a sizable fraction of the water molecules which are fully hydrogen-bonded to the nearest neighbors. On the other hand, if the hydration level decreases, mobile water molecules may find themselves in an environment where they do not form 4 hydrogen bonds with the nearest neighbors. The dynamics exhibited by such surface water molecules may no longer resemble translational jumps of water molecules in bulk or highly hydrated environments, and thus may not exhibit non-Arrhenius behavior or dynamic transition.

The idea that a sufficient average number of hydrogen bonds per water molecule may be a prerequisite for the non-Arrhenius dynamics in hydration water seems to be in agreement with a well-known fact that the onset of dynamic transition and the related bioactivity in the biomolecules does not occur below certain hydration levels.[33–35] It is likely that the dynamic transition in hydration water, which is thought to be associated with a transformation from a more developed (at low temperatures) to a less developed (at high temperatures) hydrogen bond network, simply cannot occur at low hydration levels when the average number of hydrogen bonds is insufficient to form the extensive hydrogen bond network. For such low hydration levels the dynamics may always be Arrhenius. Thus, if the dynamic transition in biomolecules is indeed triggered by the dynamic transition in the hydration water, neither transition will occur if the hydration level is too low.

It should be noted that Kittaka et al. proposed,[36] based on sorption isotherm and FTIR spectroscopic studies of sorbed water on ZnO surfaces, that the surface water coverage in this system may decrease at low temperatures due to evaporation from the oxide surface and condensation of a discrete phase elsewhere in the system, even though this suggested separate phase did not exhibit the characteristic FTIR spectrum of ice. Since bulk ice exhibits no QENS signal because of the slow relaxation times, the fact that we observe QENS broadening down to 195 K proves that sorbed water remains on the rutile nanopowder surfaces. Because the fraction of the elastic scattering in a QENS experiment always tends to grow as the temperature of the system is decreased, whether or not the total water coverage on our rutile nanoparticles decreases with decreasing temperature cannot be determined from the QENS data alone. However, this possibility will be investigated in a future QENS study over a range of total surface water coverages, coupled with classical molecular dynamics simulations at low temperatures.

4. Conclusion

The high energy resolution of the new backscattering spectrometer (BASIS) at the SNS, coupled with its broad dynamic range, has made it possible to carry out QENS measurements of the dynamics of hydration water on the surface of nanopowder rutile (α-TiO_2) down to 195 K. This is much lower than the base temperature of 250 K that could be used in the previous experiment with coarser energy resolution (DCS) at the NCNR. Based on comparison of the experimental data with the MD results, we have identified several diffusion components in the hydration water dynamics. The slowest component, attributed to chemisorbed L_1 water molecules, exhibits dynamics in the tens of nanoseconds range that is inaccessible by QENS. The slowest diffusion component

observed by QENS exhibits non-Arrhenius behavior at higher temperatures and a dynamic transition at lower temperatures and originates from the translational jumps of the fully hydrogen-bonded water molecules of the L_2 layer. A faster component, found to be of Arrhenius-type down to at least 195 K (that is, below the temperature of the dynamic transition exhibited by the slower component), is associated with the localized motions that take place in all hydration layers and require breaking fewer hydrogen bonds compared to translational jumps. Finally, an even faster component is associated with the dynamics that take place in the outermost hydration layer, L_3, where the water molecules form on average only 3 hydrogen bonds. Our findings suggest that, in order to exhibit a dynamic crossover from the low-temperature Arrhenius to the high-temperature non-Arrhenius behavior, the hydration level on the surface should be sufficiently high for a large fraction of water molecules to experience a bulk-like environment with a saturated number of hydrogen bonds to the nearest neighbor water molecules. Thus, we hypothesize that the dynamic transition in surface water may not take place at sufficiently low hydration levels.

Acknowledgment. The authors are thankful to G. Ehlers, M. Hagen, and K. Herwig for critical reading of the manuscript. We used the resources of the Computing Center for Research and Education at Vanderbilt University. Utilization of the DAVE package for the data analysis is acknowledged. This work was supported by the U.S. Department of Energy, Office of Basic Energy Sciences, Division of Chemical Sciences, Geosciences and Biosciences through the project "Nanoscale Complexity at the Oxide/Water Interface" (ERKCC41) and by Oak Ridge National Laboratory, managed by UT-Battelle, LLC, for the U.S. Department of Energy under Contract No. DE-AC05-00OR22725.

References and Notes

(1) Faraone, A.; Liu, L.; Mou, C.-Y.; Yen, C.-W.; Chen, S.-H. *J. Chem. Phys.* **2004**, *121*, 10843.

(2) Liu, L.; Chen, S-H.; Faraone, A.; Yen, C.-W.; Mou, C.-Y. *Phys. Rev. Lett.* **2005**, *95*, 117802.

(3) Liu, L.; Chen, S.-H.; Faraone, A.; Yen, C.-W.; Mou, C.-Y.; Kolesnikov, A. I.; Mamontov, E.; Leao, J. *J. Phys.: Condens. Matter* **2006**, *18*, S2261.

(4) Xu, L.; Kumar, P.; Buldyrev, S. V.; Chen, S.-H.; Poole, P. H.; Sciortino, F.; Stanley, H. E. *Proc. Nat. Acad. Sci.* **2005**, *102*, 16558.

(5) Ito, K.; Moynihan, C. T.; Angell, C. A. *Nature (London)* **1999**, *398*, 492.

(6) (a) Swenson, J. *Phys. Rev. Lett.* **2006**, *97*, 189801. (b) Cerveny, S.; Colmenero, J.; Alegria, A. *Phys. Rev. Lett.* **2006**, *97*, 189802. (c) Chen, S.-H.; Liu, L.; Faraone, A. *Phys. Rev. Lett.* **2006**, *97*, 189803.

(7) Mamontov, E.; Burnham, C. J.; Chen, S.-H.; Moravsky, A. P.; Loong, C.-K.; de Souza, N. R.; Kolesnikov, A. I. *J. Chem. Phys.* **2006**, *124*, 194703.

(8) Mamontov, E. *J. Chem. Phys.* **2005**, *123*, 171101.

(9) Mamontov, E.; Vlcek, L.; Wesolowski, D. J.; Cummings, P. T.; Wang, W.; Anovitz, L. M.; Rosenqvist, J.; Brown, C. M.; Garcia Sakai, V. *J. Phys. Chem. C* **2007**, *111*, 4328.

(10) Chen, S.-H.; Liu, L.; Fratini, E.; Baglioni, P.; Faraone, A.; Mamontov, E. *Proc. Nat. Acad. Sci.* **2006**, *103*, 9012.

(11) Chen, S.-H.; Liu, L.; Chu, X.; Zhang, Y.; Fratini, E.; Baglioni, P.; Faraone, A.; Mamontov, E. *J. Chem. Phys.* **2006**, *125*, 171103.

(12) Wang, Y.; Zhang, L.; Deng, K.; Chen, X.; Zou, Z. *J. Phys. Chem. C* **2007**, *111*, 2709.

(13) Huang, X. P.; Pan, C. X. *J. Cryst. Growth* **2007**, *306*, 117.

(14) Tahir, M. N.; Theato, P.; Oberle, P.; Melnyk, G.; Faiss, S.; Kolb, U.; Janshoff, A.; Stepputat, M.; and Tremel, W. *Langmuir* **2006**, *22*, 5209.

(15) Machesky, M. L.; Wesolowski, D. J. ; Palmer, D. A.; Ridley, M. K.; Bénézeth, P.; Lvov, S. N.; Fedkin, M. V., *Surface Complexation Modeling* (Lützenkirchen, J. ed.) Interfacial Science and Technology, Volume 11, Elsevier, Amsterdam, 324−358 (2006).

(16) Jones, P.; Hockey, J. A. *Trans. Faraday Soc.* **1971**, *67*, 2679.

(17) Zhang, Z.; Fenter, P.; Cheng, L.; Sturchio, N. C.; Bedzyk, M. J.; Predota, M.; Bandura, A.; Kubicki, J. D.; Lvov, S. N.; Cummings, P. T.; Chialvo, A. A.; Ridley, M. K.; Benezeth, P.; Anovitz, L.; Palmer, D. A.; Machesky, M. L.; Wesolowski, D. J. *Langmuir* **2004**, *20*, 4954.

(18) Fitts, J. P.; Machesky, M. L.; Wesolowski, D. J.; Shang, X.; Kubicki, J. D.; Flynn, G. W.; Heinz, T. F.; Eisenthal, K. B. *Chem. Phys. Lett.* **2005**, *411*, 399.

(19) Predota, M.; Bandura, A. V.; Cummings, P. T.; Kubicki, J. D.; Wesolowski, D. J.; Chialvo, A. A.; Machesky, M. L. *J. Phys. Chem. B* **2004**, *108*, 12049.

(20) Zhang, Z.; Fenter, P.; Sturchio, N. C.; Bedzyk, M. J.; Machesky, M. L.; Wesolowski, D. J. *Surf. Sci.* **2007**, *601*, 1129.

(21) Predota, M.; Vlcek, L. *J. Phys. Chem. B* **2007**, *111*, 1245.

(22) Herwig, K. W.; Keener, W. S. *Appl. Phys. A: Mater. Sci. Process.* **2002**, *74*, S1592.

(23) (a) For example. Swenson, J.; Bergman, R.; Howells, W. S. *J. Chem. Phys.* **2000**, *113*, 2873. (b) Swenson, J.; Bergman, R.; Longeville, S. *J. Chem. Phys.* **2001**, *115*, 11299. (c) Mamontov, E. *J. Chem. Phys.* **2004**, *121*, 9193. (d) Swenson, J.; Bergman, R.; Howells, W. S.; Longeville, S. *J. Chem. Phys.* **2004**, *121*, 9195.

(24) Russo, D.; Murarka, R. K.; Hura, G.; Verschell, E.; Copley, J. R. D.; Head-Gordon, T. *J. Phys. Chem. B* **2004**, *108*, 19885.

(25) Boerio-Goates, J.; Li, G.; Li, L.; Walker, T. F.; Parry, T.; Woodfield, B. F. *Nano Lett.* **2006**, *6*, 750.

(26) Mamontov, E. *J. Chem. Phys.* **2004**, *121*, 9087.

(27) Kuroda, Y.; Kittaka, S.; Takahara, S.; Yamaguchi, T.; Bellissent-Funel, M.-C. *J. Phys. Chem. B* **1999**, *103*, 11064.

(28) Takahara, S.; Kittaka, S.; Mori, T.; Kuroda, Y.; Yamaguchi, T.; Shibata, K. *J. Phys. Chem. B* **2002**, *106*, 5689.

(29) Mamontov, E. *J. Chem. Phys.* **2005**, *123*, 024706.

(30) Teixeira, J.; Bellissent-Funel, M.-C.; Chen, S.-H.; Dianoux, A. J. *Phys. Rev. A* **1985**, *31*, 1913.

(31) Moilanen, D. E.; Levinger, N. E.; Spry, D. B.; Fayer, M. D. *J. Am. Chem. Soc.* **2007**, *129*, 14311.

(32) Garbuio, V.; Andeani, C.; Imberti, S.; Pietropaolo, A.; Reiter, G. F.; Senesi, R.; Ricci, M. A. *J. Chem. Phys.* **2007**, *127*, 154501–1.

(33) Sokolov, A. P.; Grimm, H.; Kisliuk, A.; Dianoux, A. J. *J. Biol. Phys.* **2001**, *27*, 313.

(34) Roh, J. H.; Novikov, V. N.; Gregory, R. B.; Curtis, J. E.; Chowdhuri, Z.; Sokolov, A. P. *Phys. Rev. Lett.* **2005**, *95*, 038101.

(35) Roh, J. H.; Curtis, J. E.; Azzam, S.; Novikov, V. N.; Peral, I.; Chowdhuri, Z.; Gregory, R. B.; Sokolov, A. P. *Biophys. J.* **2006**, *91*, 2573.

(36) Kittaka, S.; Sasaki, T.; Fukuhara, N. *Langmuir* **1992**, *8*, 2598.

JP711965X